An Improved Buck-Boost Converter Suitable for PV Application

Niraj Rana*, *Student Member*, *IEEE*, Jayati Dey*, *Member*, *IEEE*, and Subrata Banerjee*, *Senior Member*, *IEEE*

*Department of Electrical Engineering, National Institute of Technology Durgapur, Durgapur-713209, India

E-mails: nirajranaosme@gmail.com, deybiswasjayati@gmail.com, bansub2004@yahoo.com

***Abstract*— In this work, an improved Input-parallel Output-series Buck-Boost converter (IOBBC) suitable for solar power generation system has been proposed and implemented. The voltage gain of IOBBC is higher than the voltage gain of the conventional Buck-Boost converter (CBBC). The closed-loop control of IOBBC has been developed with a Type-III controller. The operating performances of IOBBC have been investigated with designed controller under various conditions i.e., change in input/source voltage and change in load. It is found that the proposed IOBBC has been performed satisfactorily under the aforesaid operating conditions. The power efficiency of IOBBC has been measured and it is found that IOBBC is achieved the maximum power efficiency of 91.20%.**

Keywords*— *Conventional Buck-Boost converter (CBBC), Closed-loop control, Input-parallel Output-series Buck-Boost converter (IOBBC), Voltage gain.

I. INTRODUCTION

In the present scenario, the demand of power consumption for power production sectors is increasing day by day and available power resource is less. Therefore, power generation from non-renewable power sources is one of the attractive solution in the present case which promises reliable power generation and produces pollution free electricity for example solar based power generation system [1]-[3]. Nowadays, solar power generation attracts a great deal of attention for the users in domestic as well as in industrial sectors for pollution free production of electricity. Fig. 1 demonstrates the basic example of the solar power generation system, which mainly comprises of solar photovoltaic (PV) panel, DC-DC converter, controller and load. In the solar power generation system (Fig. 1) efficient and reliable DC-DC power converters are required to step-up the low output voltage of PV panel. At many places, conventional Buck-Boost converter (CBBC) has been integrated with MPPT controller for maximum power production from PV panel [4]. However, there are certain demerits of CBBC such as low voltage gain, poor dynamic performance and high ripple content in source current as well as in output voltage. So, the application of the aforesaid converter is restricted in some cases.

On the other hand, an isolated type DC-DC power converter may be used for generation of high voltage gain. But, due to the use of an isolated transformer in the aforesaid converter, the power handling capability as well as the power efficiency will be poor. The implemented cost and overall size of the converter will also be increased [5]. So, it's important to develop a DC-DC power converter which should have some improved qualities like high voltage gain, improved power efficiency, better dynamic response and minimum ripple.

To minimize the ripples & to improve the power efficiency, interleaving of Buck-Boost converters can be used, but overall voltage gain cannot be increased [6], [7].

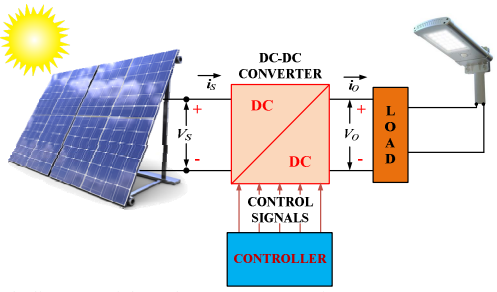

Fig. 1. Block diagram of the solar power generation system.

To increase the voltage gain and to minimize the ripples, two different high gain Input-parallel Output-series Boost converters [8], [9] have been reported in the literatures. In [8], the converter produces high voltage gain, but the converter has a disadvantage that it cannot work less than 50% duty cycle. Moreover, the aforesaid converter produces more EMI due to the lack of common ground line between the parallel-series combined converters. In [9], the converter comprises a Boost converter along with a KY-Boost converter (KYBC) [10]. The converter generates high voltage gain with low duty cycle compared to Boost converter. But, due to the use of a KYBC, the power efficiency of the aforesaid converter will be poor. The KYBC has an in-built disadvantage due to the series capacitor. The current spike through series capacitor will be high due to abruptly change of voltage across it, causing more EMI problem and undesirable power loss. Furthermore, the series capacitor will be damaged frequently. Hence, the aforementioned converter may not be suitable for some high power applications.

To overcome the aforementioned problems, an improved Input-parallel Output-series Buck-Boost converter (IOBBC) has been established in this work. The main objectives of this work are to increase the power conversion efficiency, to enhance the dynamic performance, to reduce the ripple and to attain high voltage gain of a DC-DC power converter. IOBBC exhibits a voltage gain, which is higher than the voltage gain of CBBC. The closed-loop IOBBC has been established by using '*K-factor*' based Type-III controller [11]-[13]. The dynamics performances and power efficiency of IOBBC have been investigated. It is found that the proposed IOBBC has been achieved satisfactory performances in all cases.

ISBN: 978-1-7281-4283-8 PART NO.: CFP20O01-ART

Rest of the paper is prepared as follows: Section II discusses the working principle of IOBBC. The modeling of IOBBC is demonstrated in Section III. Controller design is explained in Section IV. Simulation and experimental outcomes are illustrated in Section V. Finally, the conclusion and the useful applications of IOBBC are discussed in Section VI.

II. Proposed IOBBC

A. Power Circuit of IOBBC

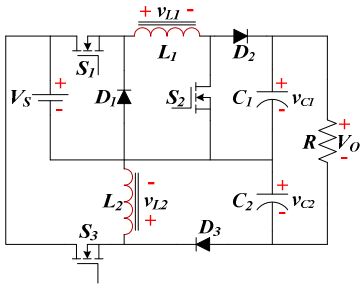

Fig. 2. Circuit topology of IOBBC.

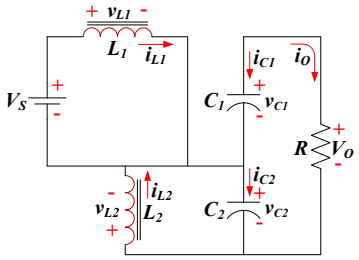

Fig. 3. Equivalent circuit of IOBBC in Mode-I.

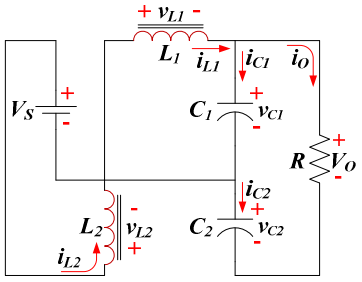

Fig. 4. Equivalent circuit of IOBBC in Mode-II.

The circuit topology of IOBBC is demonstrated in Fig. 2. The proposed IOBBC comprises of two different CBBCs. The parallel connection is applied in source side along with series connection is utilized in load side of two CBBCs. The parallel-series combination of CBBCs operates in an interleaving operation (i.e., 180° phase shifting operation) during one complete switching period with identical duty cycle. In this way, the ripple in the output voltage along with the source current of IOBBC will be diminished as well as voltage gain of the said converter will also be amplified. The power circuit elements of IOBBC are as follows: inductors (L_1 & L_2), capacitors (C_1 & C_2), switches (S_1, S_2 & S_3), diodes (D_1, D_2, & D_3) & load resistor (R). V_S and V_O are the source and output voltages respectively. v_{L1}, v_{L2}, v_{C1} & v_{C2} are the voltage across L_1, L_2, C_1 & C_2 respectively. Under continuous conduction mode (CCM) operation, IOBBC operates in two different operating modes (Mode-I and Mode-II). The corresponding equivalent circuits of IOBBC during Mode-I and Mode-II are shown in Fig. 3 and Fig. 4 respectively. As per the operating modes, the time-domain waveforms of inductors current (i_{L1} & i_{L2}), inductors voltage (v_{L1} & v_{L2}), capacitors current (i_{C1} & i_{C2}) and gate drive signals of switches (V_{sw1}, V_{sw2} & V_{sw3}) of proposed IOBBC are given in Fig. 5, where, δ_1 & δ_2 are the duty cycle of the respective converters and T is the total switching duration.

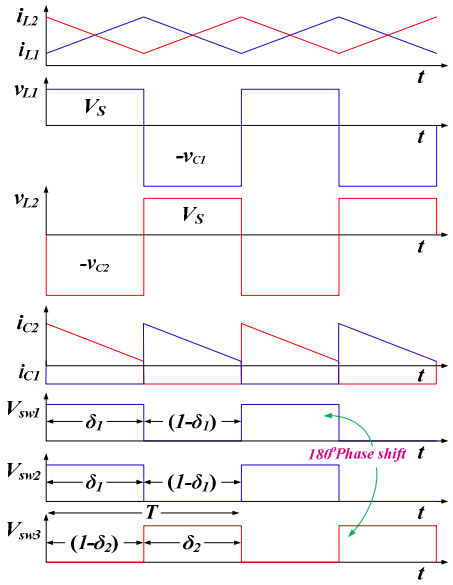

Fig. 5. Theoretical time-domain waveforms of inductors current (i_{L1} & i_{L2}), inductors voltage (v_{L1} & v_{L2}), capacitors current (i_{C1} & i_{C2}) and gate drive signals of switches (V_{sw1}, V_{sw2} & V_{sw3}) of IOBBC.

B. Steady-state voltage gain

The voltage equations of inductors and capacitors of IOBBC during Mode-I operation can be deduced by using KVL in the circuit demonstrated in Fig. 3 and are given below.

$$v_{L1} = V_S \;;\quad v_{L2} = -v_{C2} \;;\quad V_O = v_{C1} + v_{C2} \tag{1}$$

Similarly, by utilizing KVL in the circuit demonstrated in Fig. 4, the voltage equations of inductors and capacitors of IOBBC during Mode-II operation are established as follows.

$$v_{L1} = -v_{C1} \;;\quad v_{L2} = V_S \;;\quad V_O = v_{C1} + v_{C2} \tag{2}$$

From the time-domain waveform (shown in Fig. 5) of V_{L1} and by applying equal volt-sec principle across L_1, one can deduced (3).

$$v_{C1} = \delta_1 V_S / (1 - \delta_1) \tag{3}$$

From the time-domain waveform (shown in Fig. 5) of V_{L2} and by using equal volt-sec principle across L_2, (4) is derived.

$$v_{C2} = \delta_2 V_S / (1 - \delta_2) \tag{4}$$

Now, it is assumed that $\delta_1 = \delta_2 = \delta$ and the phase difference between δ_1 & δ_2 is 180°. Therefore, by adding (3) & (4), the final voltage gain expression (5) of IOBBC is derived as follows

$$V_O / V_S = 2\delta / (1 - \delta) \tag{5}$$

In the case of CBBC, the voltage gain expression can be written as follows

$$V_O / V_S = \delta / (1 - \delta) \tag{6}$$

From (5) and (6), it is appeared that IOBBC generates two times higher voltage gain than the voltage gain of CBBC.

ISBN: 978-1-7281-4283-8

PART NO.: CFP20O01-ART

C. Current gain

When power losses of IOBBC are neglected then the power input (P_{in}) is equal to the power output (P_O) and it is illustrated in (7).

$$P_{in} = P_O \Rightarrow V_S i_S = V_O i_O \tag{7}$$

Therefore, the current gain expression can be derived as follows.

$$i_O / i_S = (1-\delta)/2\delta \tag{8}$$

where, i_S and i_O are the currents flowing through source & load of IOBBC.

D. Inductors design

The inductors (L_1 & L_2) value of IOBBC for CCM operation can be selected by using the following equation (9).

$$(L_1 = L_2) > \frac{1}{4} RT(1-\delta)^2 \tag{9}$$

E. Capacitors design

The output filter capacitors (C_1 & C_2) can be selected based on the following equation (10).

$$C_1 = \frac{\delta T V_O}{R \Delta v_{C1}} \; ; \qquad C_2 = \frac{\delta T V_O}{R \Delta v_{C2}} \tag{10}$$

III. Modeling of IOBBC

IOBBC has two operating modes (Mode-I and Mode-II) in CCM operation. Therefore, the state equations of IOBBC during Mode-I (Fig. 3) can be written as follows.

$$\frac{di_{L1}}{dt} = \frac{V_S}{L_1} \; ; \qquad \frac{di_{L2}}{dt} = \frac{-v_{C2}}{L_2} \tag{11}$$

$$\frac{dv_{C1}}{dt} = \frac{-V_O}{RC_1} \; ; \qquad \frac{dv_{C2}}{dt} = \frac{i_{L2}}{C_2} - \frac{V_O}{RC_2} \tag{12}$$

And, when IOBBC operates in Mode-II (Fig. 4), then the state equations are as follows.

$$\frac{di_{L1}}{dt} = \frac{-v_{C1}}{L_1} \; ; \qquad \frac{di_{L2}}{dt} = \frac{V_S}{L_2} \tag{13}$$

$$\frac{dv_{C1}}{dt} = \frac{i_{L1}}{C_1} - \frac{V_O}{RC_1} \; ; \qquad \frac{dv_{C2}}{dt} = \frac{-V_O}{RC_2} \tag{14}$$

The average state equations of IOBBC are derived after considering $\delta_1 = \delta_2 = \delta$ and are given in (15)-(18).

$$\frac{di_{L1}}{dt} = \frac{V_S}{L_1}\delta - \frac{v_{C1}}{L_1}(1-\delta) \tag{15}$$

$$\frac{di_{L2}}{dt} = \frac{V_S}{L_2}\delta - \frac{v_{C2}}{L_2}(1-\delta) \tag{16}$$

$$\frac{dv_{C1}}{dt} = \frac{-V_O}{RC_1}\delta + \left(\frac{i_{L1}}{C_1} - \frac{V_O}{RC_1}\right)(1-\delta) \tag{17}$$

$$\frac{dv_{C2}}{dt} = \frac{-V_O}{RC_2}\delta + \left(\frac{i_{L2}}{C_2} - \frac{V_O}{RC_2}\right)(1-\delta) \tag{18}$$

After solving equations (15)-(18), the control-to-output transfer function of IOBBC has been established and it is presented in (19).

$$\frac{V_O(s)}{\delta(s)} = \frac{2V_S}{(1-\delta)^2} \times \frac{\left\{1 - \frac{2\delta L}{R(1-\delta)^2} s\right\}}{\left\{\frac{LC}{(1-\delta)^2} s^2 + \frac{2L}{R(1-\delta)^2} s + 1\right\}} \tag{19}$$

where, $L = L_1 = L_2$ and $C = C_1 = C_2$.

TABLE-I: Parameters of IOBBC

Sl. No.	Parameters	Value
1	Source Voltage (V_S)	36V
2	Output Voltage (V_O)	20-100V
3	Inductors (L_1 & L_2)	250µH
4	Capacitors (C_1 & C_2)	470µF
5	Load (R)	30-100Ω
6	Switching frequency (f_s)	50kHz

The power circuit parameters for simulation and experimental analyses of IOBBC are summarized in Table-I. These parameters are selected based on the fundamental design equations which are given in section II. After putting parameters values into (19), the final transfer function ($V_O(s)/\delta(s)$) of IOBBC for a specific working state (V_O = 100V, R = 100Ω) is derived in (20).

$$\frac{V_O(s)}{\delta(s)} = \frac{-10165\left(s - 6.028\times10^4\right)}{\left(s^2 + 42.55s + 1.491\times10^6\right)} \tag{20}$$

The above transfer function (20) has been utilized to establish a Type-III controller for closed-loop IOBBC.

IV. Controller Design

The controller parameters play an important role for obtaining better dynamic response and performances. Accordingly, in this work, a Type-III controller has been designed for IOBBC based on '*K-factor*' approach to accomplish better stability characteristics in closed-loop. Type-III controller is cascade combination of 'lead-lead' controllers with one pole at zero position. So, the controller can produce maximum 180° 'phase-lead' with zero steady-state error.

The generalized transfer function of Type-III controller is given in (21)

$$G_C(s) = \frac{(1+s/\omega_z)^2}{(s/\omega_{p0})(1+s/\omega_p)^2} \tag{21}$$

where, ω_z, ω_{p0} & ω_p are the frequencies of double zero, pole at zero position and double pole of the controller ($G_C(s)$).

The magnitude of $G_C(s)$ can be written as

$$\left|G_C(j\omega)\right| = \frac{\left|(1+j\omega/\omega_z)^2\right|}{\left|(j\omega/\omega_{p0})\right|\left|(1+j\omega/\omega_p)^2\right|} \tag{22}$$

The argument of $G_C(s)$ can be derived as

$$\angle G_C(j\omega) = 2\tan^{-1}(\omega/\omega_z) - 2\tan^{-1}(\omega/\omega_p) - \frac{\pi}{2} \tag{23}$$

Now, taking derivative of (23) w.r.t frequency (f) maximum 'phase-lead' can be derived.

$$\frac{d}{df}\left(\angle G_C(j\omega)\right) = \frac{d}{df}\left(2\tan^{-1}(f/f_z) - 2\tan^{-1}(f/f_p)\right) \tag{24}$$

After solving 'f' from (24), the maximum 'phase-lead' can be accomplished at 'geometric-mean' of double zero & double pole frequency of the controller.

$$f_{\max} = \sqrt{f_z \times f_p} \tag{25}$$

Hence, f_{max} is taken as crossover-frequency (f_c) of Type-III controller.

Now, presenting '*K-factor*' of Type-III controller and it can be written as the ratio between f_p to f_z. Therefore, the relationship can be derived between 'phase-lead' and 'K' as follows.

$$'phase-lead' = 2\tan^{-1}\sqrt{K} - 2\tan^{-1}\left(1/\sqrt{K}\right) \tag{26}$$

And, 'K' can be derived from (26) as follows.

$$K = \left\{\tan\left(\frac{'phase-lead'}{4} + \frac{\pi}{4}\right)\right\}^2 \tag{27}$$

Equation (27) is known as '*K-factor*' of Type-III controller.

Hence, f_z and f_p location can be found from (28) for a particular crossover-frequency (f_c) and required 'phase-lead'.

$$f_z = f_c/\sqrt{K}\ ; \qquad f_p = f_c \times \sqrt{K} \tag{28}$$

Now, it is supposed that the converter has -12 dB gain deficit at f_c = 1 kHz and required 'phase-lead' is 160°. From (28), the location of f_z & f_p are calculated and are given in (29).

$$f_z = 87.49Hz\ ; \qquad f_p = 11.43kHz \tag{29}$$

At 1 kHz chosen 'f_c', gain (G) must be -12dB. Consequently, 0-dB crossover pole location is established as follows.

$$f_{p0} = \frac{Gf_z\left(f_p^2 + f_c^2\right)}{f_p^2\left(\sqrt{\left(\frac{f_z}{f_c}\right)^2 + 1}\right)\left(\sqrt{\left(\frac{f_c}{f_z}\right)^2 + 1}\right)} = 30.46Hz \tag{30}$$

After fine tuning of gain, zero and pole locations, the final transfer function of the controller ($G_C(s)$) is obtained and it is illustrated in (31).

$$G_C(s) = \frac{18667(s+468.7)^2}{s(s+61000)^2} \tag{31}$$

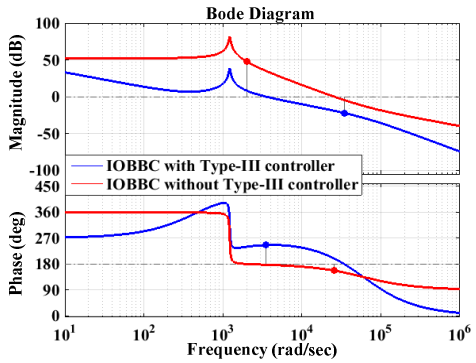

Fig. 6. Bode plot of IOBBC with and without Type-III controller.

The closed-loop performance of IOBBC has been studied in frequency response analysis and a Bode plot has also been established with and without Type-III controller, which is shown in Fig. 6. The closed-loop performance specifications are listed in Table-II. From the analysis, it is found that IOBBC with designed controller demonstrates superior stability performance.

TABLE-II: CLOSED-LOOP PERFORMANCE OF IOBBC

Specifications	Value
Gain Margin	22.1 dB
Phase Margin	65.7°
Gain Crossover Frequency	3540 rad/sec
Phase Crossover Frequency	34400 rad/sec

V. SIMULATION AND EXPERIMENTAL RESULTS

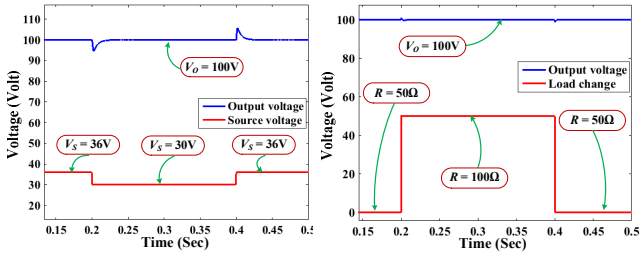

(a) (b)

Fig. 7. Output voltage (V_O) response of IOBBC against (a) change in source voltage (V_S) and (b) change in load (R).

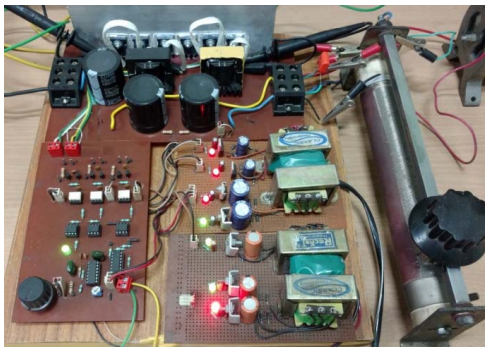

Fig. 8. Prototype picture of IOBBC.

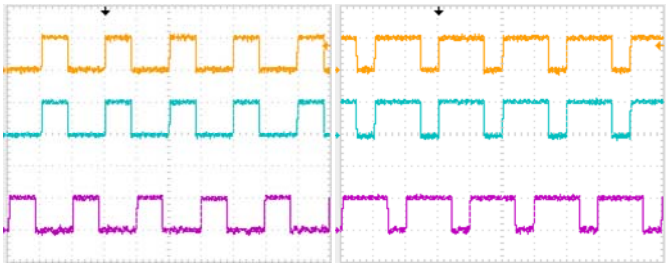

(a) (b)

Fig. 9. Experimental gate drive signals for switches (S_1, S_2 & S_3) of IOBBC during (a) Buck mode (b) Boost mode.

To verify the stability characteristics of proposed IOBBC with developed controller extensive analysis has been performed under various cases i.e., change in input/source voltage and change in load. The transient responses of the output voltage of IOBBC have been captured by changing of source voltage and by changing of load, which are presented in Fig. 7(a) & (b) respectively. It is clear that in both cases, IOBBC exhibits superior and robust performance.

The prototype fabrication of closed-loop IOBBC with developed controller has been carried out in the laboratory. The whole circuitry has been constructed in a single PCB and the

ISBN: 978-1-7281-4283-8

PART NO.: CFP20O01-ART

prototype picture of IOBBC is illustrated in Fig. 8. The experimental gate drive signals for three power switches (S_1, S_2 & S_3) of IOBBC during Buck & Boost modes are shown in Fig. 9(a) & (b). Here, gate drive signals for switches (S_1 & S_2) are equal and are in the same phase. However, the gate drive signal for switch (S_3) is 180° out of phase w.r.t other two switches (S_1 & S_2). The experimental steady-state waveforms of inductors current (i_{L1} & i_{L2}) along with gate drive signals for switches (S_1 & S_3) of IOBBC in Buck and Boost modes are demonstrated in Fig. 10(a) & (b). The experimental steady-state waveforms of source voltage (V_S) and output voltage (V_O) of IOBBC during Buck and Boost modes are illustrated in Fig. 11(a) & (b). The power efficiency of IOBBC has been measured against the output power and a graph is plotted between efficiency (%) vs. output power (W) and it is illustrated in Fig. 12. It appears that IOBBC is achieved the maximum power efficiency of 91.20%.

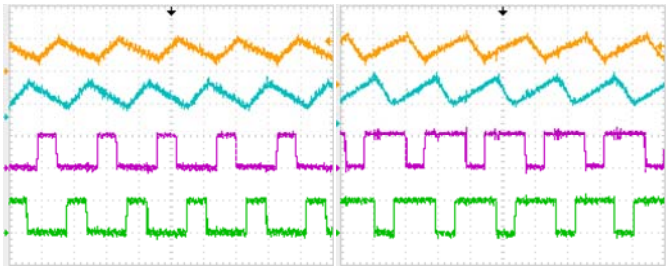

(a) (b)

Fig. 10. Experimental steady-state waveforms of inductors current (i_{L1} & i_{L2}), along with gate drive signals for switches (S_1 & S_3) of IOBBC during (a) Buck mode (b) Boost mode.

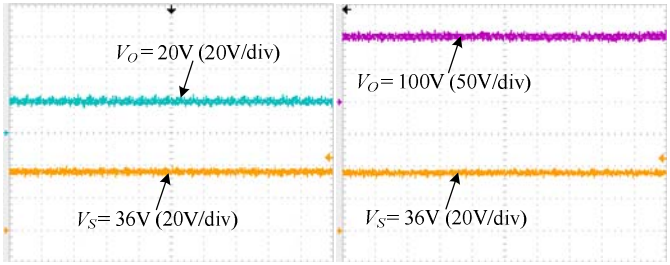

(a) (b)

Fig. 11. Experimental steady-state waveforms of source voltage (V_S) and output voltage (V_O) of IOBBC during (a) Buck mode (b) Boost mode.

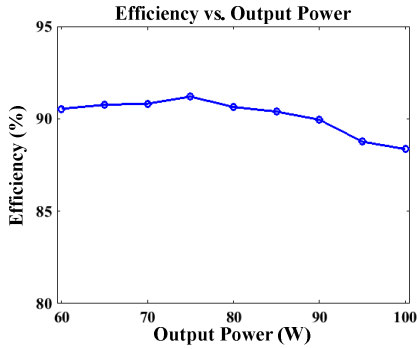

Fig. 12. Efficiency (%) vs. output power (W) of IOBBC.

VI. Conclusion

An improved IOBBC suitable for solar power generation system has been proposed and established in this work. The effectiveness of the proposed converter is established through analysis, simulation and experimental results. From the results, some certain advantages of proposed IOBBC can be concluded, e.g., high voltage gain, improved stability & performance in closed-loop and enhanced power efficiency. The merits of proposed IOBBC is beneficial for the integration with some practical applications based on solar power generation systems like solar powered electric vehicles, solar powered irrigation systems, photovoltaic based water pumping system, solar power LED street light, solar tree etc.

References

[1] J. Adhikari, A. K. Rathore, and S. K. Panda, "Modular Interleaved Soft-Switching DC-DC Converter for High-Altitude Wind Energy Application," *IEEE Journal of Emerging and Selected Topics in Power Electronics*, vol. 2, no. 4, pp. 727-738, Dec. 2014.

[2] M. Forouzesh, Y. Shen, K. Yari, Y. P. Siwakoti, and F. Blaabjerg, "High-Efficiency High Step-Up DC-DC Converter With Dual Coupled Inductors for Grid-Connected Photovoltaic Systems," *IEEE Transactions on Power Electronics*, vol. 33, no. 7, pp. 5967-5982, Jul. 2018.

[3] S. K. Rathor, A. Patel, S. Patel, and J. Patel, "Closed loop buck-boost converter using RTW," in *proc. International Conference on Electrical, Electronics, and Optimization Techniques (ICEEOT)*, 2016.

[4] C.-L. Shen, and P.-C. Chiu, "Buck-boost-flyback integrated converter with single switch to achieve high voltage gain for PV or fuel-cell applications," *IET Power Electronics*, vol. 9, no. 6, pp. 1228-1237, May 2016.

[5] A. Chub, D. Vinnikov, R. Kosenko, and E. Liivik, "Wide Input Voltage Range Photovoltaic Microconverter with Reconfigurable Buck-Boost Switching Stage," *IEEE Transactions on Industrial Electronics*, vol. 64, no. 7, pp. 5974-5983, Jul. 2017.

[6] T.-R. G.-Luna, I. A.-Vargas, A. J. Forsyth, K. C.-Pulido, P. V.-Elizondo, I. Cervantes, F. G.-Olguin, and A. V.-Parra, "Two-phase, Dual Interleaved Buck-Boost DC-DC Converter for Automotive Applications," *IEEE Transactions on Industry Applications*, Sep. 2019, DOI: 10.1109/TIA.2019.2942026.

[7] G. Sivanagaraju, S. Samata, L. M. Kunzler, K. R. Feistel, A. K. Rathore, and L. A. Lopes, "PFC Interleaved Buck-Boost Converter for Telecom Power Application," in *proc. 43rd Annual Conference of the IEEE Industrial Electronics Society (IECON 2017)*, pp. 2299-2304, Dec. 2017.

[8] X. Hu, and C. Gong, "A High Gain Input-Parallel Output-Series DC/DC Converter with Dual Coupled Inductors," *IEEE Transactions on Power Electronics*, vol. 30, no. 3, pp. 1306-1317, Mar. 2015.

[9] P. Wang, L. Zhou, Y. Zhang, J. Li, and M. Sumner, "Input-Parallel Output-Series DC-DC Boost Converter With a Wide Input Voltage Range, For Fuel Cell Vehicles," *IEEE Transactions on Vehicular Technology*, vol. 66, no. 9, pp. 7771-7781, Sep. 2017.

[10] K. I. Hwu, Y. H. Chen, and W. C. Tu, "Negative-Output KY Boost Converter," *IEEE International Symposium on Industrial Electronics (ISIE 2009)*, Seoul Olympic Parktel, Seoul, Korea, pp. 272-274, Jul. 2009.

[11] N. Rana, A. Ghosh, and S. Banerjee, "Development of an Improved Tri-State Buck-Boost Converter with Optimized Type-3 Controller," *IEEE Journal of Emerging and Selected Topics in Power Electronics*, vol. 6, no. 1, pp. 400-415, Mar. 2018.

[12] N. Rana, M. Kumar, A. Ghosh, and S. Banerjee, "A Novel Interleaved Tri-state Boost Converter with Lower Ripple and Improved Dynamic Response," *IEEE Transactions on Industrial Electronics*, vol. 65, no. 7, pp. 5456-5465, Jul. 2018.

[13] N. Rana, and S. Banerjee, "Development of an Improved Input-Parallel Output-Series Buck-Boost Converter and Its Closed-Loop Control," *IEEE Transactions on Industrial Electronics*, Sep. 2019, DOI: 10.1109/TIE.2019.2938482.